# Enhancement of $PbZrO_3$ polarization using a Ti seed layer for energy storage application

Mamadou D. Coulibaly , Caroline Borderon , Raphaël Renoud , Hartmut W. Gundel

PII: S0040-6090(20)30640-4
DOI: https://doi.org/10.1016/j.tsf.2020.138432
Reference: TSF 138432

To appear in: *Thin Solid Films*

Received date: 18 June 2020
Revised date: 29 October 2020
Accepted date: 7 November 2020

Please cite this article as: Mamadou D. Coulibaly , Caroline Borderon , Raphaël Renoud , Hartmut W. Gundel , Enhancement of $PbZrO_3$ polarization using a Ti seed layer for energy storage application, *Thin Solid Films* (2020), doi: https://doi.org/10.1016/j.tsf.2020.138432

# Enhancement of $PbZrO_3$ polarization using a Ti seed layer for energy storage application

Mamadou D. Coulibaly[1,*], Caroline Borderon[1], Raphaël Renoud[1] and Hartmut W. Gundel[1]

[1] *IETR UMR CNRS 6164, University of Nantes, 2 Rue de la Houssinière, 44322 Nantes, France*

*corresponding author e-mail: mamadoucoulibalypro1@gmail.com

Keywords

Antiferroelectric, Energy storage, Lead zirconate, Sol-gel deposition, Titanium seed layer.

HIGHLIGHTS

- Reduction of lattice mismatch on alumina polycrystalline substrate
- Enhancement of $PbZrO_3$ polarization is achieved by using a Ti seed layer
- The (111) $PbZrO_3$ presents an increase of 56 % of the polarization compared to the (100) $PbZrO_3$
- A higher recoverable energy density is obtained in the (111) $PbZrO_3$ (8 J/cm$^3$)

Abstract - Enhancement of lead zirconate ($PbZrO_3$) polarization is achieved by using a titanium seed layer on alumina polycrystalline substrate. Thanks to the reduction of the lattice mismatch between the platinum electrode (3.92 Å) and the $PbZrO_3$ films (4.14 Å), lead zirconate thin films oriented along the (111) direction with an orientation factor of around 65 % has been obtained. The (111) $PbZrO_3$ presents an increase of 56 % of the polarization compared to the (100) $PbZrO_3$. This enhancement is responsible of the higher recoverable energy storage density obtained in the (111) $PbZrO_3$ thin films (8 J/cm$^3$ at 600 kV/cm with an efficiency of 72 %). The (111) $PbZrO_3$ also has a higher figure of merit, which indicates that the (111) crystallographic plane is the most favorable direction for energy storage.

## Introduction

The study of thin film capacitor for energy storage application is receiving more and more attention due to the growing demand for autonomous and wireless sensors[1],[2]. Advantages of thin film capacitors are a high energy density with a low footprint [3],[4] and the security of the device since it is entirely solid [5]. Among the dielectric materials, antiferroelectric $PbZrO_3$ thin films are the most widely used for energy

polarization.

Previous works on single crystal substrates have shown the influence of a thin titanium seed layer (< 5 nm) on the crystallographic orientation of $PbZrO_3$ thin films [6],[7]. This allows controlling the dipole orientation and hence the material's dielectric properties. In this study, the lead zirconate crystallographic orientation is optimized while using an alumina polycrystalline substrate. This optimization should lead to a significant reduction of the production cost since monocrystalline substrates represent an important part of the device price.

Experimental procedure

The $PbZrO_3$ thin films are prepared by a sol-gel process. Lead acetate trihydrate $[Pb(CH_3CO_2)_2.3H_2O]$ with 10 % molar excess is dissolved in deionized water and acetic acid, the water/acetic acid molar ratio is 85/15. Acetic acid is introduced at a rate of 1 ml per 1.2 g of lead acetate. An excess of lead is used in order to compensate the loss during the annealing treatment due to the formation of the volatile PbO [8]. Zirconium isopropoxide $[Zr(O(CH_2)_2CH_3)_4]$ is then added to the solution. In addition, Ethylene glycol [HO-$CH_2$-$CH_2$OH] is used at a rate of 1 mL per 7.5 g of lead acetate, in order to reduce the appearance of cracks [9] in the film and improves the solution stability [10]. The concentration of the final solution is 0.5 M. The precursor solution is then deposited on a polished alumina substrate precoated with a 40 nm titanium adhesion layer and a 300 nm platinum bottom layer done by magnetron sputtering. Twelve layers have been deposited at 4000 rpm during 25 s by a multi-step spin coating process and each layer is annealed during 10 min in a pre-heated open air furnace at 650 °C. The overall films thickness is 800 nm. Square platinum electrodes of 0.5 mm broad are deposited by RF magnetron sputtering in order to realize a Metal-Insulator-Metal capacitor. To study the influence of a titanium seed layer on the crystallographic orientation of the $PbZrO_3$ layers, 1 nm, 2 nm and 3 nm of titanium are deposited by sputtering before the $PbZrO_3$ layers (Fig. 1). The thickness of titanium is calculated according to the deposition rate of the sputtering process.

The cross-sectional morphology of the films is examined with a *Jeol 7600* scanning electron microscope (SEM) at an accelerating voltage of 5 kV. The structure and phase purity of the films are analyzed using a *Bruker D8*X- ray diffractometer (XRD) with Cu$K\alpha$ radiation and the Bragg-Brentano configuration. The

pol[illegible]er

Tower circuit and the energy storage performance is calculated according to the (*P–E*) results. The current - electric field hysteresis loops are obtained thanks to a modified Sawyer Tower circuit by replacing the sense capacitor by a resistor of 100 Ω. The capacitance and the dielectric losses (tan $\delta$) are measured with an *Agilent 4294A*, the relative permittivity of each sample is calculated from the measured capacitance.

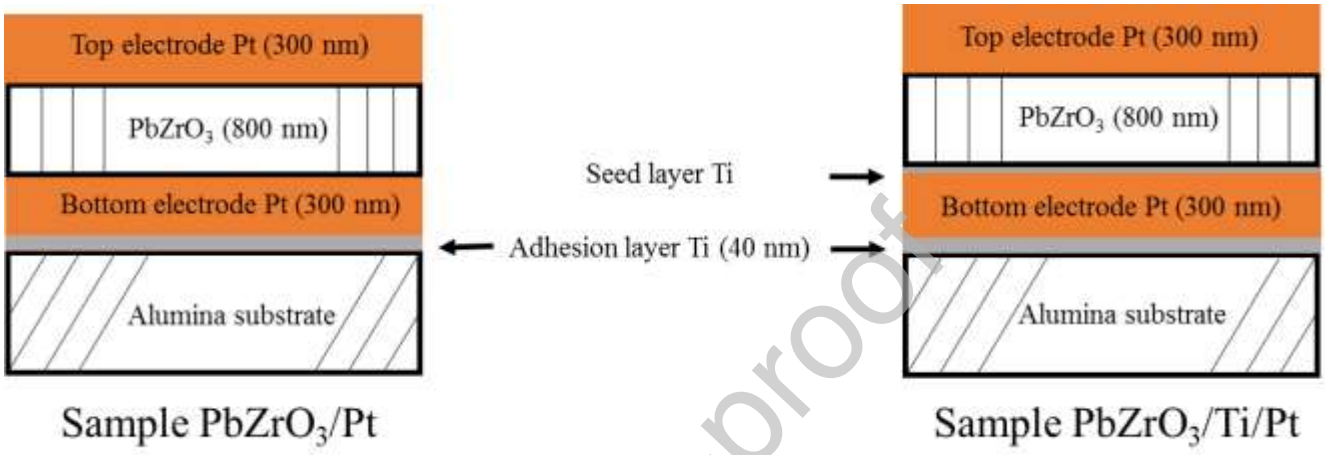


Fig. 1. Schematic diagram of the MIM capacitors for the different structures



## Results and discussion

### A. Structural properties

The X-ray diffraction patterns of the $PbZrO_3$ thin films are shown in Fig. 2 with the indices of the pseudocubic perovskite structure. All samples are well crystallized and no parasitic pyrochlore phase is found.

The orientation factor ($\alpha_{hkl}$) can be calculated for each peak thanks to the following equation [11],[12] :

$$\alpha_{hkl} = \frac{I_{hkl}}{I_{total}} \times 100 \, , \qquad (1)$$

where $I_{hkl}$ corresponds to the peak intensity of the selected plane and $I_{total}$ is the sum of all diffraction peaks.

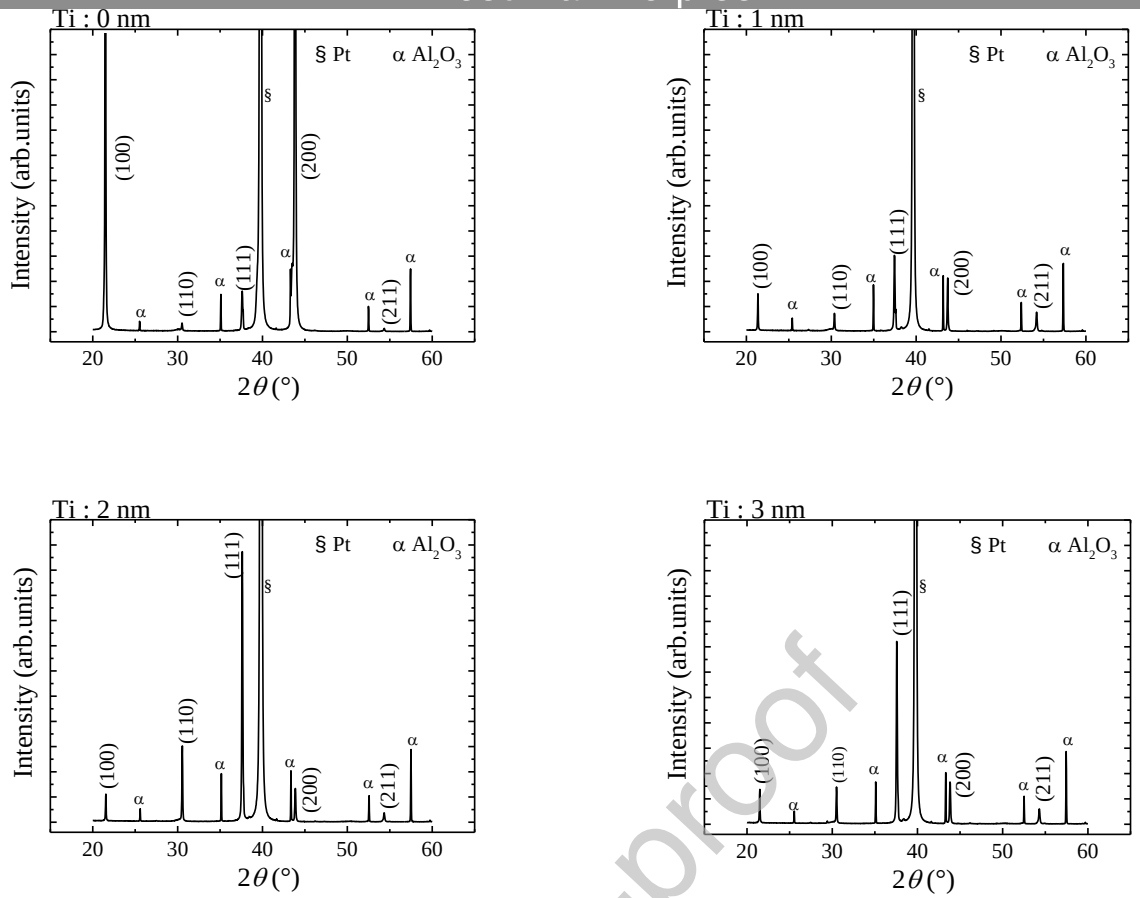


Fig 2. X-ray diffraction patterns of the lead zirconate thin films with different thickness of titanium seed layer

The sample with no titanium seed layer (Ti: 0 nm) is oriented along the (100) crystallographic plane at around 99 % which is similar to what is obtained when single crystal substrate is used [6]. This orientation on smooth polycrystalline alumina substrate is due to a most thermodynamically favorable growth direction [13],[14] on a lowest surface energy [7]. Contrary to this sample, a (111) preferential orientation is obtained at 65 % when introducing 2 nm of Ti seed layer, which is in agreement with the work of Muralt et *al.* [6]. During the crystallization, the titanium seed layer forms an intermetallic ($Pt_3Ti$) layer with the platinum bottom electrode [7],[15], reducing the lattice mismatch between the Pt electrode (3.92 Å) and the $PbZrO_3$ films (4.14 Å). This intermetallic layer facilitates the $PbZrO_3$ growth in the (111) crystallographic direction on the highly (111) oriented platinum bottom electrode. However, when using 1 nm and 3 nm of Ti seed layer, less oriented materials are obtained (at 37 % and 58.5 % respectively).

been calculated using the main planes (111), (110) and (100) (Fig. 3). The $I_{111}/I_{100}$ ratio shows that the maximum orientation along (111) is obtained with 2 nm of Ti which corresponds to what we observed in the XRD pattern. This ratio is closed to zero for the sample with no seed layer due to the highly (100) oriented $PbZrO_3$. A similar evolution is observed for the $I_{110}/I_{100}$ ratio, which shows that the use of the titanium seed layer also promotes a slightly growth of the (110) $PbZrO_3$ plane, but the texture in this orientation is less pronounced compared to the (111) direction. Therefore, the evolution of the $I_{111}/I_{110}$ ratio is quite stable, indicating a constant growth of the (111) texture in relation to the (110) plane.

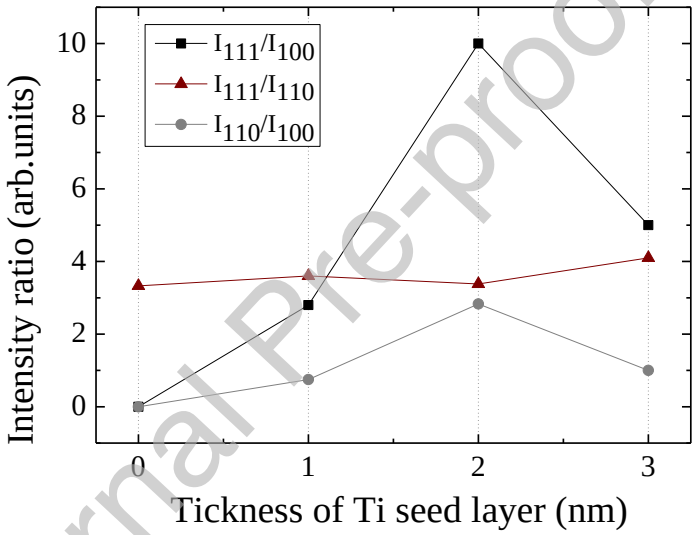


Fig. 3. Evolution of the diffraction intensity ratios as a function of the Ti seed layer thickness

Fig.4 shows cross-sectional SEM morphology of the (100) and (111) oriented lead zirconate. Both samples have a similar columnar like structure and all films are uniform and crack-free. Due to the multicoating deposition process of the $PbZrO_3$, layer interfaces could clearly be observed. In the (111) $PbZrO_3$, the Ti seed layer cannot be seen because of the formation of the thin intermetallic $Pt_3Ti$ layer during the crystallization. The thickness of the film and of one layer is respectively 800 nm and 70 nm for all samples.

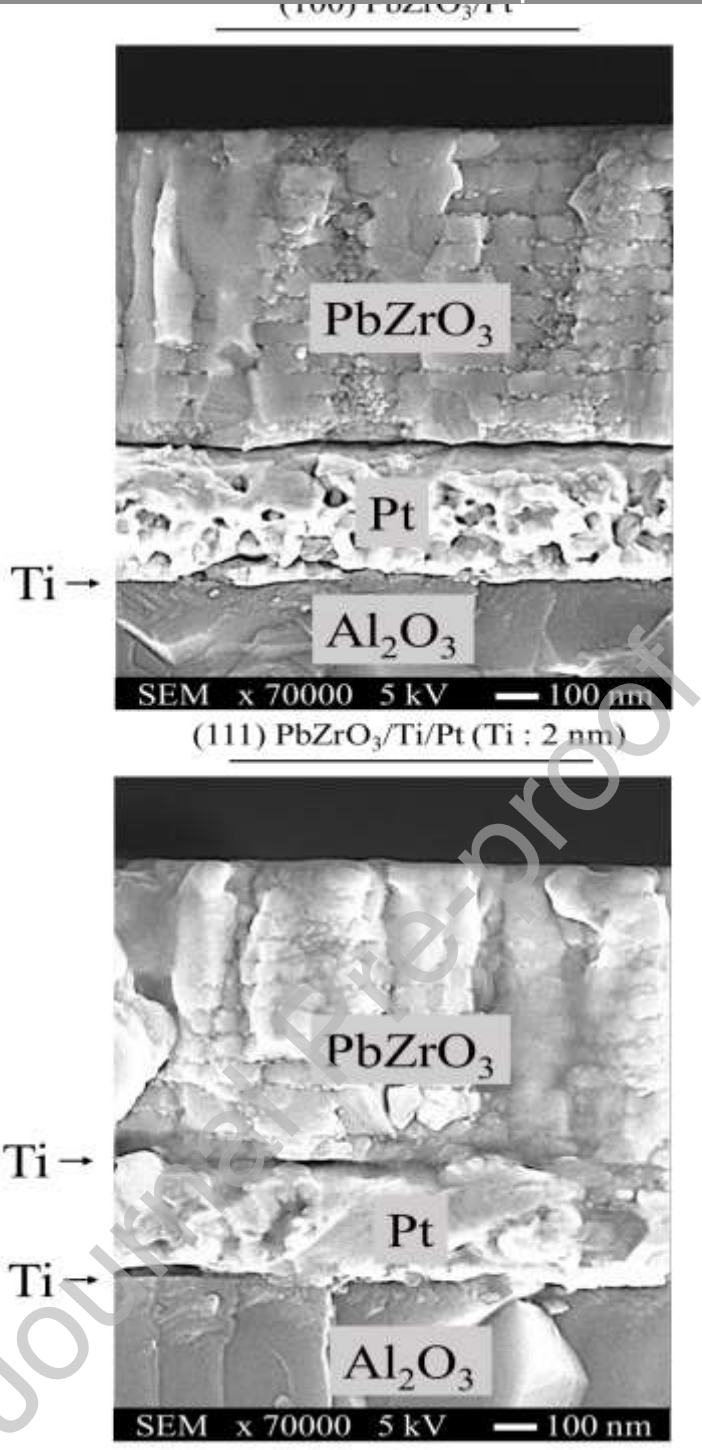


Fig. 4. Cross-sectional SEM morphology of (100) and (111) $PbZrO_3$

B. Dielectric properties

Polarization loops of the lead zirconate thin films at 600 kV/cm are shown in the Fig.5. All films have developed double hysteresis loops, indicating their antiferroelectric nature. The sample which is oriented along the (111) direction (Ti: 2 nm) has the higher maximum polarization (36 $\mu C/cm^2$) while the (100) $PbZrO_3$ (Ti: 0 nm) has the lowest polarization (23 $\mu C/cm^2$) at 600 kV/cm. For the less oriented materials, Ti:

1 n[illegible] ts can be explained by the modification of the polar axis orientation. For $PbZrO_3$ thin films with a (111) orientation, the angle between the applied electric field and the [111] polar axis ($\vec{P}_{FE}$) of the ferroelectric rhombohedral phase is lower compared to the (100) $PbZrO_3$ [7],[16] (Fig. 6). Thus, for the (111) $PbZrO_3$ films the energy necessary to align the dipoles in the direction of the electric field is smaller compared to the (100) $PbZrO_3$. Therefore, more the orientation factor along the (111) direction is high, more the polarization is important. The polar direction ($\vec{P}_{AFE}$) of the antiferroelectric tetragonal cell which is along the [110] axis has less effect on the dielectric properties of the material because in this state, the elementary dipoles are anti-parallels [17].

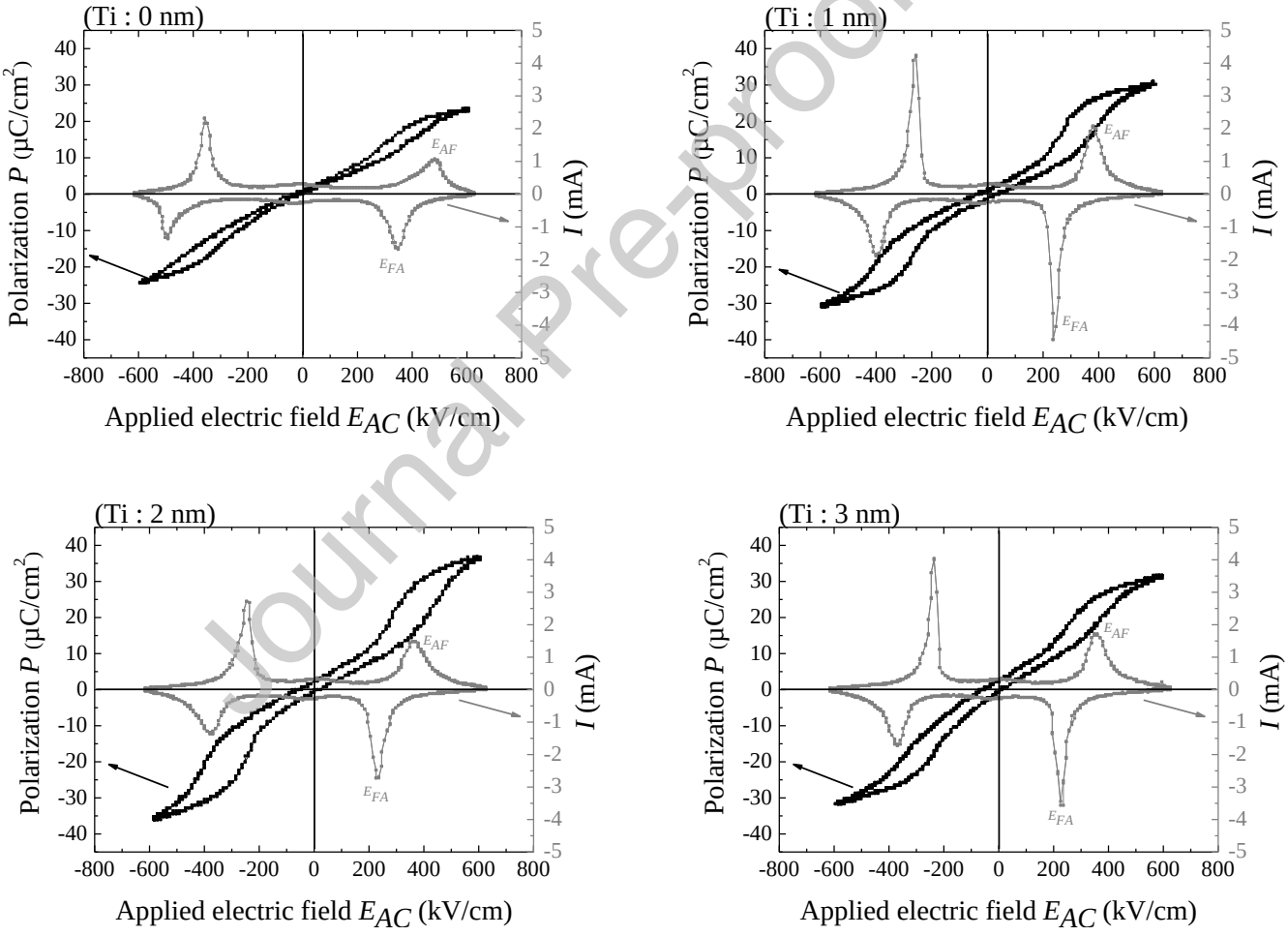


Fig. 5. Polarization and current – electric hysteresis loops of the lead zirconate thin films as function of Ti seed layer thickness at 1kHz. $E_{AF}$ and $E_{FA}$ are the transitions fields.

(111) $PbZrO_3$ (Ti: 2 nm) has the lowest antiferroelectric-ferroelectric field transition ($E_{AF}$ = 350 kV/cm) and the (100) $PbZrO_3$ has the highest one ($E_{AF}$ = 490 kV/cm). The ferroelectric-antiferroelectric fields transitions ($E_{FA}$) are also influenced by the crystallographic orientation of the material, it is induced by the reduction of the angle between the applied electric field and the ferroelectric polar axis ($\vec{P}_{FE}$). As a result, the (111) lead zirconate is easier to polarize compared to the (100) $PbZrO_3$. For the same reason, the (111) $PbZrO_3$ has a lower ferroelectric-antiferroelectric transition field ($E_{FA}$ = 230 kV/cm) than the (100) $PbZrO_3$ ($E_{FA}$ = 350 kV/cm).

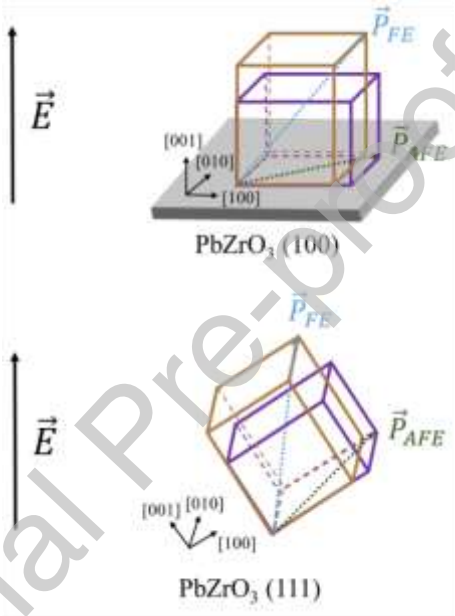


Fig. 6. Schematic diagram of the primitive cells for the

(100) and (111) oriented $PbZrO_3$

Polarization is important for energy storage performances as the recoverable energy density ($W$) stored in the capacitor can be calculated from the discharge branch of the polarization loop (Fig.7) by [18]:

$$W = \int_0^{P_{Sat}} EdP \qquad (2)$$

The energy storage efficiency ($\eta$) can be obtained by considering the energy consumed ($W_L$) during the discharge [18]:

$$\eta = \frac{W}{W + W_L} \quad (3)$$

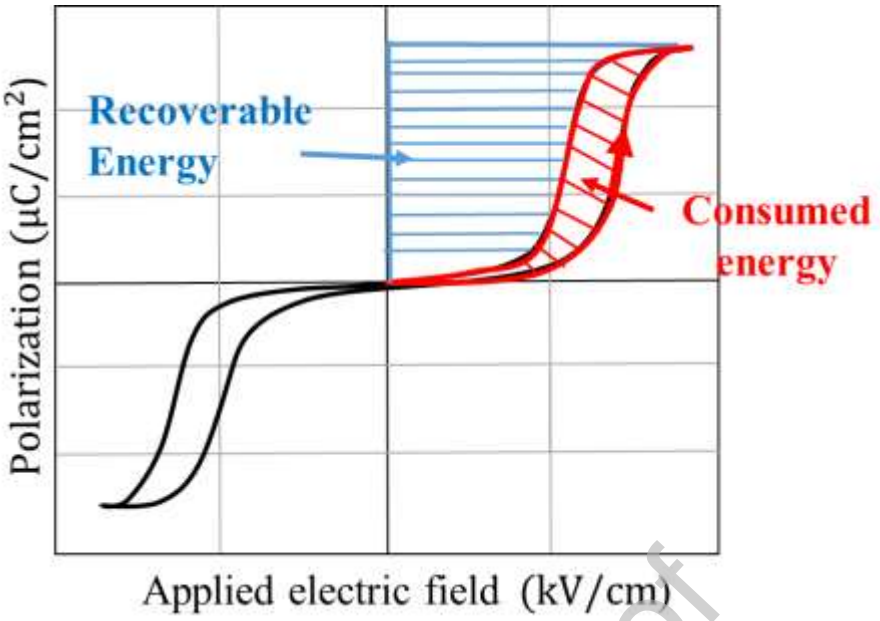


Fig.7. Schematic presentation of the stored energy in an antiferroelectric polarization cycle

The recoverable energy stored is higher for the (111) $PbZrO_3$ (Ti: 2 nm), which is in accord with the higher polarization of the (111) $PbZrO_3$ (Fig.8). Due to low polarization, the (100) $PbZrO_3$ (Ti: 0 nm) and less oriented materials have lower energy densities. A high polarization is necessary to obtain a large energy stored.

The (111) $PbZrO_3$ presents a recoverable energy density of (8 J/cm$^3$) with an efficiency of 72 %, which is similar to what is reported in (111) $PbZrO_3$ [3] deposited on $SrTiO_3$ single crystal. This shows that the use of a single crystal substrate is not mandatory for the development of an energy storage device and can be replaced by a low cost alumina polycrystalline substrate without damaging its properties.

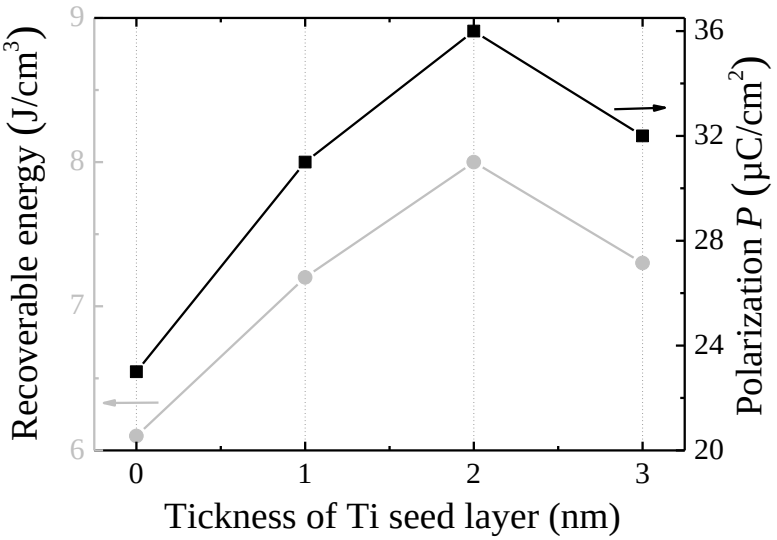


Fig.8. Recoverable energy stored and the polarization as function of the titanium seed layer thickness at 600 kV/cm.

On the other hand, the (100) $PbZrO_3$ ($\eta$ = 82 %) has a higher efficiency compared to the (111) $PbZrO_3$ ($\eta$ = 72 %). This higher efficiency is related to its slimmer polarization loop, which is characteristic of a material with low dielectric losses.

In order to determine which of the crystallographic orientations is the most favorable for energy storage, a figure of merit (F.O.M.) is calculated [4].

$$F.O.M = W \times \eta \qquad (4)$$

A F.O.M. of 5.75 J/cm$^3$ is obtained for the (111) $PbZrO_3$ (Ti: 2 nm), while the (100) $PbZrO_3$ has a F.O.M. of 5 J/cm$^3$. This shows that the (111) crystallographic plane is the most favorable direction for energy storage.

are presented in Fig. 9. The (111) $PbZrO_3$ (Ti: 2 nm) has the higher relative permittivity ($\varepsilon_r$' ≈ 155 at 1 kHz) while the (100) $PbZrO_3$ (Ti: 0 nm) has the lowest value ($\varepsilon_r$' ≈ 137 at 1 kHz). The high permittivity observed in (111) $PbZrO_3$ can be explained by the easy rotation and incline of domain and polar vectors in this texture due to a highly *c*-axis material [19]. Zhao et *al*. [11] have reported a same evolution in lead zirconate antiferroelectric films.

All samples have low dielectric losses (tan $\delta$ < 0.02). Nevertheless, dielectric losses are slightly higher for samples using a Ti seed layer, which explains their lower efficiencies. This phenomenon is related to the oxidation of the Ti seed layer, which induces a raise of the dielectric losses. Indeed, titanium has a poor oxidation stability [20],[14] in the crystallization conditions of lead zirconate (≈ 650 °C) and induces the generation of oxygen vacancies in the lead zirconate structure [21].

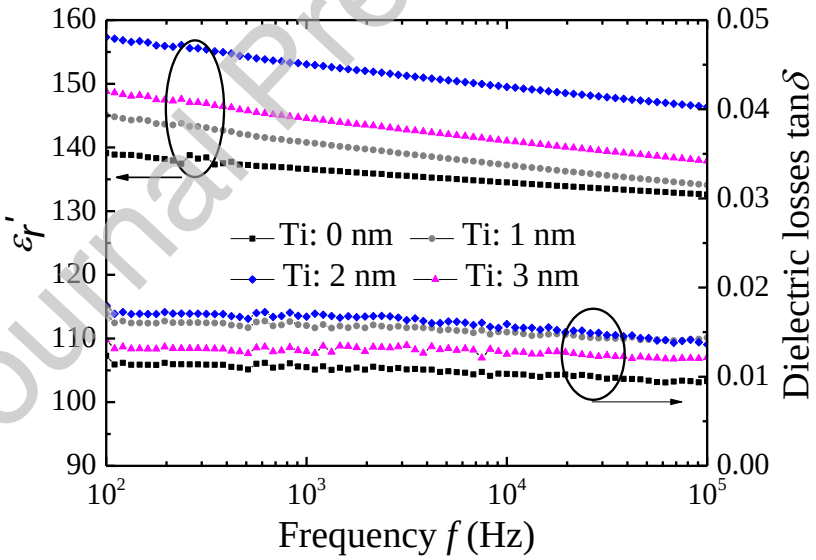


Fig. 9. Real part of relative permittivity and dielectric losses as a function of frequency of the lead zirconate thin films for different Ti seed layer thickness

## Conclusion

Optimization of lead zirconate ($PbZrO_3$) polarization by using titanium seed layer has been investigated. Thanks to the reduction of the lattice mismatch between the platinum electrode (3.92 Å) and the $PbZrO_3$ films (4.14 Å), lead zirconate thin films oriented along the (111) direction on an alumina polycrystalline substrate has been grown. The sample with 2 nm of titanium seed layer presents an orientation factor of around 65 % along the (111) plane, which shows that the modification of lead zirconate crystallographic orientation is possible even when using a polycrystalline substrate. This optimization leads to the control of the $PbZrO_3$ crystallographic growth without having recourse of an expensive monocrystalline substrate which is an important achievement in order to optimize dielectric and energy storage properties in a low cost way.

The (111) $PbZrO_3$ has a higher maximum polarization (36 $\mu C/cm^2$) compared to the (100) $PbZrO_3$ saturation polarization (23 $\mu C/cm^2$) at 600 kV/cm. These results can be explained by the modification of the polar axis direction when the crystallographic orientation is modified. When the $PbZrO_3$ has a (111) orientation, the angle between the applied electric field and the [111] polar axis of the ferroelectric rhombohedral phase is lower compared to the (100) $PbZrO_3$. Enhancement of the polarization also contributes to the amelioration of the energy storage performances. The recoverable energy density (8 $J/cm^3$) obtained for the (111) $PbZrO_3$ is higher than the (100) $PbZrO_3$ density (6 $J/cm^3$), which indicates that (111) crystallographic orientation is more suitable for an energy storage application. The calculation of F.O.M confirms this result. Nevertheless, samples using a Ti seed layer present higher dielectric losses, which is due to the titanium weak oxidation stability in the crystallization conditions (≈ 650 °C).

Mamadou D. Coulibaly : Conceptualization, Methodology, Writing - Review & Editing

Caroline Borderon : Supervision, Writing - Review & Editing,

Raphaël Renoud : Supervision, Visualization

Hartmut W. Gundel : Supervision, Visualization

**Declaration of interests**

☒ The authors declare that they have no known competing financial interests or personal relationships that could have appeared to influence the work reported in this paper.

☐The authors declare the following financial interests/personal relationships which may be considered as potential competing interests:



References

[1] R. Md. Ferdous, A. W. Reza, M. F. Siddiqui, Renewable energy harvesting for wireless sensors using passive RFID tag technology: A review, Renew. Sustain. Energy Rev. 58 (2016) 1114‑1128, https://doi.org/10.1016/j.rser.2015.12.332.

[2] F. K. Shaikh, S. Zeadally, Energy harvesting in wireless sensor networks: A comprehensive review, Renew. Sustain. Energy Rev. 55 (2016) 1041‑1054, https://doi.org/10.1016/j.rser.2015.11.010.

[3] [illegible] gy storage in epitaxial $PbZrO_3$ antiferroelectric films using strain engineering, Appl. Phys. Lett. 105 (2014) 112908, https://doi.org/10.1063/1.4896156.

[4] C. Borderon, K. Nadaud, M. Coulibaly, R. Renoud, H. Gundel, Mn-Doped $Ba_{0.8}Sr_{0.2}TiO_3$ Thin Films for Energy Storage Capacitors, Int. J. Adv. Res. Phys. Sci. 6 (2019) 1‑9.

[5] F. Wang, Y. Wang, Development and Utilization of Integral Thin Film Capacitors, Procedia Environ. Sci. 18 (2013) 871‑874, https://doi.org/10.1016/j.proenv.2013.04.117.

[6] P. Muralt, T. Maeder, L. Sagalowicz, S. Hiboux, Texture control of $PbTiO_3$ and $Pb(Zr,Ti)O_3$ thin films with $TiO_2$ seeding, J. Appl. Phys. 83 (1998) 3835‑3841, https://doi.org/10.1063/1.366614.

[7] T. Tani, J. Li, D. Viehland, D. A. Payne, Antiferroelectric- ferroelectric switching and induced strains for sol- gel derived lead zirconate thin layers, J. Appl. Phys. 75 (1994) 3017‑3023, https://doi.org/10.1063/1.356146.

[8] C. K. Kwok, S. B. Desu, Pyrochlore to perovskite phase transformation in sol-gel derived lead-zirconate-titanate thin films, Appl. Phys. Lett. 60 (1992) 1430-1432, https://doi.org/10.1063/1.107312.

[9] S. Yu, K. Yao, S. Shannigrahi, F. T. E. Hock, Effects of poly(ethylene glycol) additive molecular weight on the microstructure and properties of sol-gel-derived lead zirconate titanate thin films, J. Mater. Res. 18 (2003) 737‑741, https://doi.org/10.1557/JMR.2003.0100.

[10] G. Yi, M. Sayer, An acetic acid/water based sol-gel PZT process I: Modification of Zr and Ti alkoxides with acetic acid, J. Sol-Gel Sci. Technol. 6 (1996) 65–74, https://doi.org/10.1007/BF00402590.

[11] Y. Zhao, H. Gao, X. Hao, Q. Zhang, Orientation-dependent energy-storage performance and electrocaloric effect in PLZST antiferroelectric thick films, Mater. Res. Bull. 84 (2016). 177‑184, https://doi.org/10.1016/j.materresbull.2016.08.005.

[12] W. Zhu, W. Ren, H. Xin, P. Shi, X. Wu, Enhanced ferroelectric properties of highly (100) oriented Pb ( $Zr_{0.52}Ti_{0.48}$)$O_3$ thick films prepared by chemical solution deposition, J. Adv. Dielectr. 3 (2013) 1350011, https://doi.org/10.1142/S2010135X13500112.

[13] [illegible] 1-μm-thick lead zirconate titanate film fabricated by a double-spin-coating process, Appl. Phys. Lett. 85 (2004) 2322‑2324, https://doi.org/10.1063/1.1794354.

[14] K. G. Brooks, I. M. Reaney, R. Klissurska, Y. Huang, L. Bursill, N. Setter, Orientation of rapid thermally annealed lead zirconate titanate thin films on (111) Pt substrates, J. Mater. Res. 9 (1994) 2540‑2553, https://doi.org/10.1557/JMR.1994.2540.

[15] S.-Y. Chen, I.-W. Chen, Texture development, microstructure evolution, and crystallization of chemically derived PZT thin films, J. Am. Ceram. Soc. 81 (1998) 97–105, https://doi.org/10.1111/j.1151-2916.1998.tb02300.x.

[16] J. Ge, D. Remiens, J. Costecalde, Y. Chen, X. Dong, and G. Wang, Effect of residual stress on energy storage property in $PbZrO_3$ antiferroelectric thin films with different orientations, Appl. Phys. Lett. 103 (2013) 162903, https://doi.org/10.1063/1.4825336.

[17] B. Xu, Y. Ye, and L. E. Cross, « Dielectric properties and field-induced phase switching of lead zirconate titanate stannate antiferroelectric thick films on silicon substrates », J. Appl. Phys., vol. 87, no 5, p. 2507‑2515, mars 2000, doi: 10.1063/1.372211.

[18] X. Hao, J. Zhai, L. B. Kong, and Z. Xu, « A comprehensive review on the progress of lead zirconate-based antiferroelectric materials », Prog. Mater. Sci., vol. 63, p. 1‑57, juin 2014, doi: 10.1016/j.pmatsci.2014.01.002.

[19] Liu, Y., Yang, X., He, C., Li, X., Wang, Z., Xiao, Y., and Long, X., « Domain and antiferroelectric properties of Pb(Lu 1/2 Nb 1/2 )O 3 single crystals and their superlattice structure », RSC Adv, vol. 7, no 7, p. 3704‑3712, 2017, doi: 10.1039/C6RA26171J.

[20] K. Sreenivas, I. Reaney, T. Maeder, N. Setter, C. Jagadish, and R. G. Elliman, « Investigation of Pt/Ti bilayer metallization on silicon for ferroelectric thin film integration », J. Appl. Phys., vol. 75, no 1, p. 232‑239, janv. 1994, doi: 10.1063/1.355889.

[21] [illegible] on the dielectric properties of PbZrO 3 thin films," Appl. Phys. Lett., vol. 117, no. 14, p. 142905, Oct. 2020, doi: 10.1063/5.0017984.

List of figures